Supporting Information

Enhancement of inflection point focusing and rare-cell separations from untreated whole blood

*Dongwoo Lee, Yo-han Choi, and Wonhee Lee**

Supporting Display items

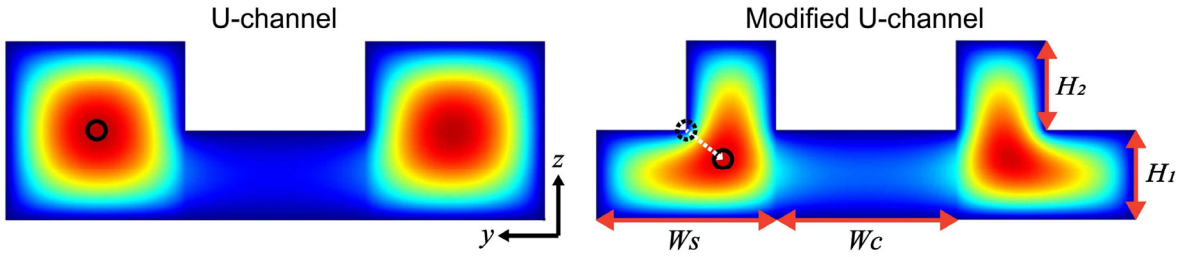

Figure S1. Channel cross-section.

We have tested several device designs that can lead to inflection point focusing. Simple U-channels (Figure S1, left) and modified U-channels (Figure S1, right) are prepared with varying dimensions. Figure S1 shows two representative channel cross-sections and the velocity field within the channels. The black circles are the locations of the velocity maxima for each case. For the U-channel, the velocity maximum is located almost at the center of the side channel. In the modified U-channel, the location of the velocity maximum can be shifted downwards and toward the channel center, which helps increase the shear rate and the lift force within the center channel. In addition, the modified U-channel design enables us to reduce the amount of fluid flowing in the side channel. The flow rate in the side channels is ~ 3/4 times smaller for the modified U-channel compared to the simple U-channel when the maximum velocities are the same.

We wanted the device to work best for particles with diameters of ~10-15 μm. For W_c, a smaller value is preferred to achieve a higher focusing efficiency by reducing the distance of the particle migration toward the inflection points. However, a smaller W_c resulted in an unstable co-flow and poor separation purity. In addition, a small H_1 and W_c lead to lower throughput. We varied H_1 and W_c from 30- 200 μm, and they were determined to be 50 and 100 μm to achieve a relatively stable co-flow without seriously sacrificing the throughput and focusing efficiency. H_2 and W_s were determined to be 50 and 100 μm, respectively. A change in these dimensions does not significantly change the overall focusing efficiency. They are more closely related to the flow rate required in the side channel. A larger H_2 and W_s lead to a larger flow rate in the side channel to achieve the same level of focusing efficiency. We believe further investigation and optimization of the dimensions and the flow conditions will enable better performance in focusing and separation. In the current study, the cross-sectional dimensions of the device were fixed to the values given above.

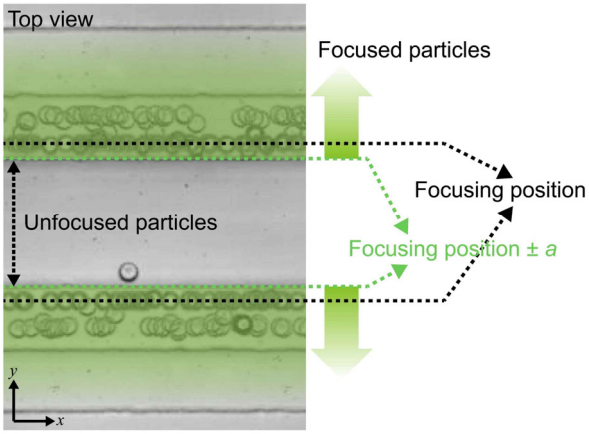

Figure S2. Schematic for the efficiency calculation of the particle focusing.

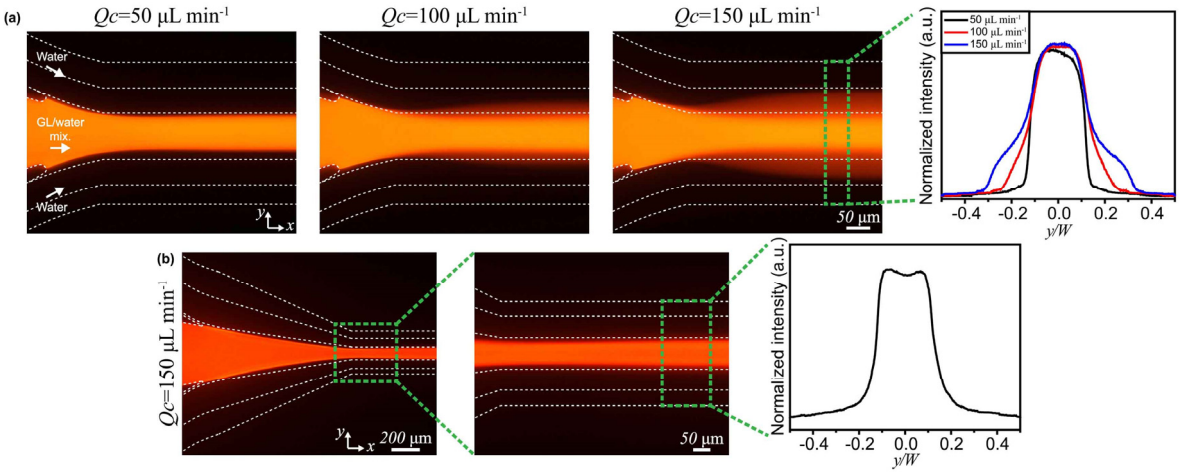

Figure S3. Disturbed co-flow boundary due to secondary flow. (a) Fluorescent images and normalized fluorescent intensities where the inlets merges. With the flow rate increased, disturbance of the co-flow boundaries became noticeable. Large mismatch in flow speed resulted in secondary flows. At high flow rate of 150 μL min^{-1}, the boundary of the two liquids became noticeably broader from the top view. (b) Fluorescent images after balancing the velocities between the side flow and the center flow by modifying the channel design (flow rate of 150 μL min^{-1}). The normalized fluorescence intensity from the magnified image shows sharp drop indicating secondary flow mixing is insignificantly small.

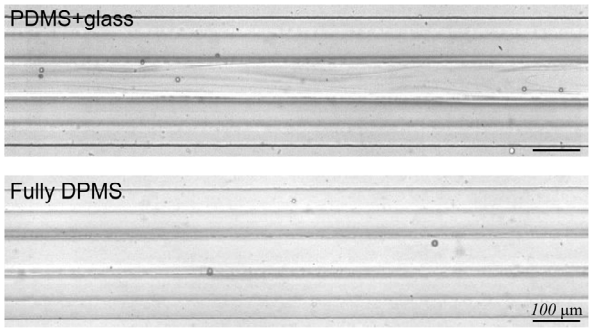

Figure S4. Stability of co-flows depending on channel material. Unstable fluid boundaries were observed in PDMS-glass microchannels when the flow rate was high (> ~ 100 μL/min). Such instability was removed by replacing the bottom surface as PDMS.

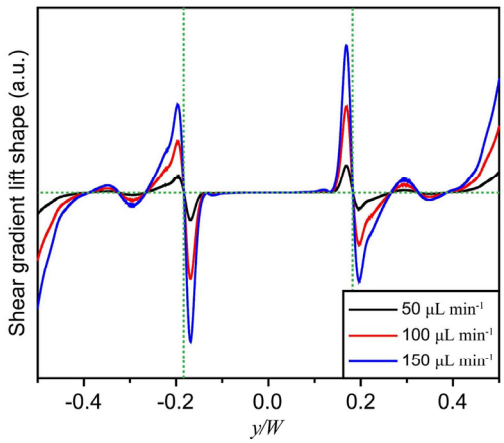

Figure S5. Shear gradient lift shapes calculated from flow speed simulation for each flow rate condition.

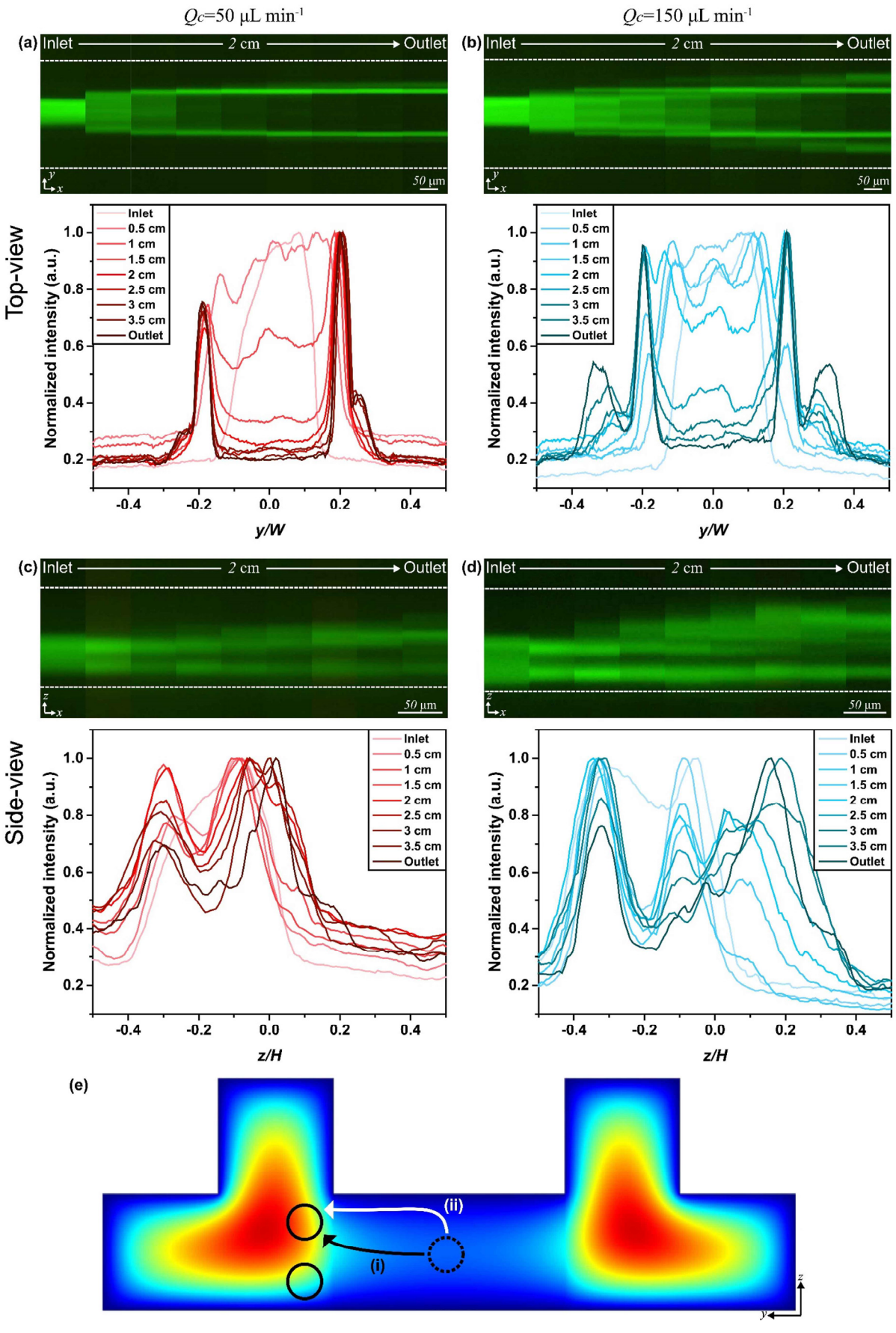
Qc=50 μL min-1
Qc=150 μL min-1
(a)
(b)
Inlet
2 cm
Outlet
50 μm
Top-view
Side-view
Normalized intensity (a.u.)
y/W
z/H
Inlet
0.5 cm
1 cm
1.5 cm
2 cm
2.5 cm
3 cm
3.5 cm
Outlet
(c)
(d)
(e)
(i)
(ii)

Figure S6. Comparison of particle trajectories in a low flow rate (Q_c=50 µL min^{-1}) and a high flow rate (Q_c=150 µL min^{-1}) conditions. Fluorescent images were taken from the top-view (a and b) and side-view (c and d) with an interval of 0.5 cm from the inlet to the outlet. The normalized fluorescent intensities were plotted. (e) Major particle migration route to the inflection point for different flow rates: (i) Q_c=50 µL min^{-1} and (ii) Q_c=150 µL min^{-1}.

The trajectories of the particle migration for the low (Q_c = 50 µL min^{-1}) and the high (Q_c = 150 µL min^{-1}) flow rate conditions were investigated by fluorescent imaging from the top- and side-view to find out whether the pathway of the particle migration affected the focusing efficiencies (Figure S6). We obtained the images at intervals of 0.5 cm from the inlet to the outlet. The 15.5 µm fluorescent particles were used. From the top-view images, it is clear that the particles migrate toward the inflection points faster in the low flow rate condition than in the high flow rate condition, which agrees with the statistical results in Figure 4 (Figure S6a and S6b). However, from the side-view images, it was found that the particles migrate faster toward the top and bottom walls in the high flow rate condition compared to the low flow rate condition (Figure S6c and S6d). In other words, when the flow rate is high enough, the ratio of particles moving toward the top and bottom walls increases, and resultantly, the particles migrate toward the inflection points slowly due to the weak shear gradient lift force near the walls (Figure S6e).

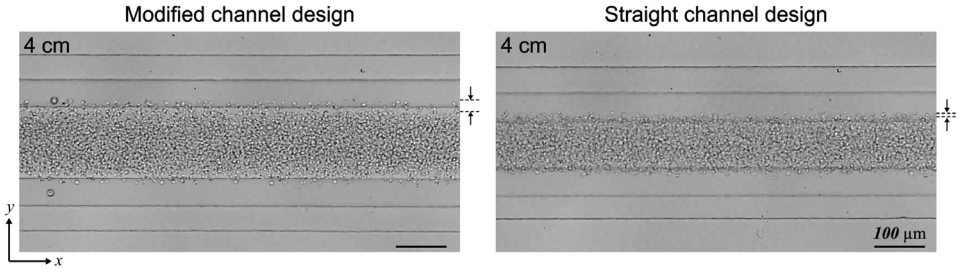

Figure S7. High-speed images of blood/DPBS co-flows to show difference in the width of blood stream in the modified channel and the original straight channel.

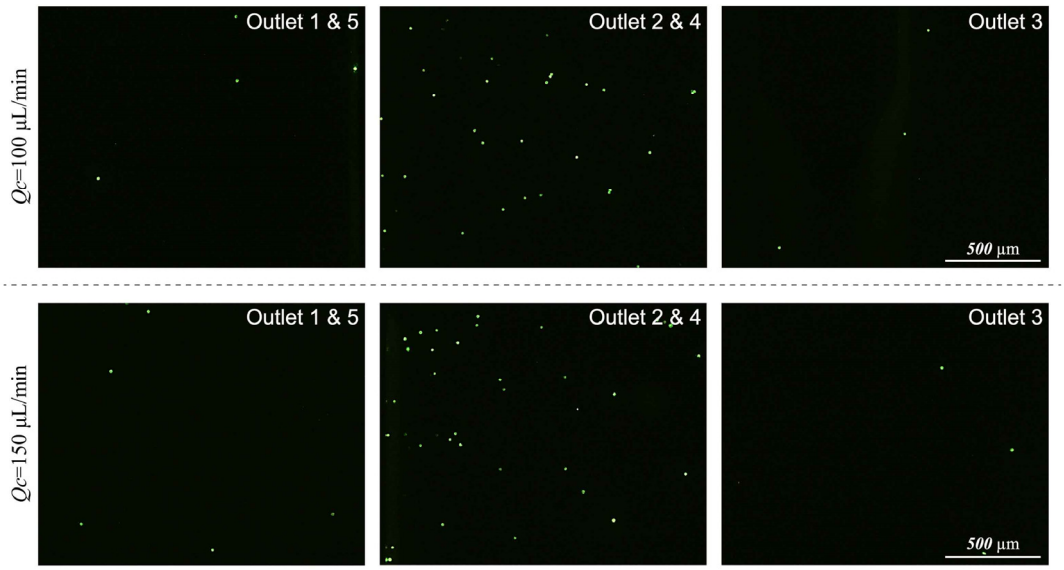

Figure S8. Fluorescent images for HeLa cells collected from each outlet with Q_cs = 100 µl min^{-1} and 150 µl min^{-1}.